Probing the complex loading dependent structural changes in ultra-high drug loaded polymer micelles by small-angle neutron scattering

Benedikt Sochor[1,+], Özgür Düdükcü[1,+], Michael M. Lübtow[2], Bernhard Schummer[3], Sebastian Jaksch[4], Robert Luxenhofer[2,5*]

[1] *Chair of X-Ray Microscopy, Department of Physics and Astronomy, University Würzburg, Campus Hubland Nord, Josef-Martin-Weg 63, 97074 Würzburg, Germany*

[2] *Functional Polymer Materials, Chair for Advanced Materials Synthesis, Department of Chemistry and Pharmacy and Bavarian Polymer Institute, University of Würzburg, Röntgenring 11, 97070 Würzburg, Germany*

[3] *Fraunhofer Institute for Integrated Circuits, X-Ray Development Center EZRT, Flugplatzstraße 75, 90768 Fürth, Germany*

[4] *Forschungszentrum Jülich GmbH, Jülich Center for Neutron Science (JCNS) at Heinz Maier-Leibnitz Zentrum, Lichtenberstraße 1, 85747 Garching, Germany*

[5] *Soft Matter Chemistry, Department of Chemistry, Helsinki University, 00014 Helsinki, Finland*

[+] authors contributed equally
[*]correspondence to: robert.luxenhofer@uni-wuerzburg.de

Keywords: nanomedicine, nanoformulations, drug solubilization, drug-polymer interaction, drug-corona interactions

ABSTRACT: Drug loaded polymer micelles or nanoparticles are being continuously explored in the fields of drug delivery and nanomedicine. Commonly, a simple core-shell structure is assumed, in which the core incorporates the drug and the corona provides steric shielding, colloidal stability, and prevents protein adsorption. Recently, the interactions of the dissolved drug with the micellar corona have received increasing attention. Here, using small-angle neutron scattering, we provide an in-depth study of the differences in polymer micelle morphology of a small selection of structurally closely related polymer micelles at different loadings with the model compound curcumin. This work supports a previous study using solid state nuclear magnetic resonance spectroscopy and we confirm that the drug resides predominantly in the core of the micelle at low drug loading. As the drug loading increases, neutron scattering data suggests that an inner shell is formed, which we interpret as the corona also starting to incorporate the drug, whereas the outer shell mainly contains water and the polymer. The presented data clearly shows that a better understanding of the inner morphology and the impact of the hydrophilic block can be important parameters for improved drug loading in polymer micelles as well as provide insights into structure-property relationships.

1. INTRODUCTION

Promising new active pharmaceutical ingredients (API) are discovered in pharmaceutical industry and academia on a daily basis, but one major challenge remains the formulation of the API. According to estimates, 40%[1] - 60%[2] of all new drugs are practically insoluble in water. Therefore, a plethora of methods is used to increase their solubility.[3] Polymer micelles are nanoscopic structures formed by amphiphilic (block) copolymers.[4] In a simplified picture, hydrophobic APIs are dissolved in the hydrophobic core, whereas the hydrophilic shell acts as a protective layer to prevent premature disintegration or unwanted protein interactions and to ensure a sufficient water solubility. However, the actual situation may be more complex as recently shown for a variety of drug loaded micelles, as the nature of the hydrophobic block can significantly affect the drug loading.[5, 6] A particularly strong effect was reported for the different solubilization behaviors of structurally very similar poly(2-oxazoline) (POx) and poly(2-oxazine) (POzi) based drug delivery vehicles (Scheme 1).

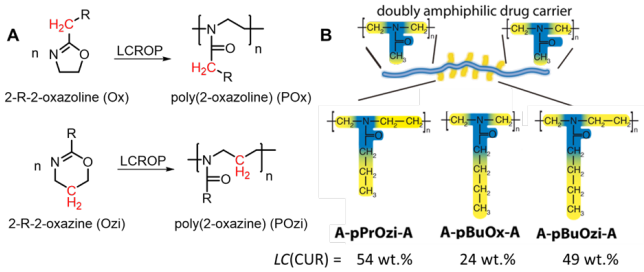

Scheme 1: A) Schematic synthesis of the structural isomers poly(2-oxazoline)s (POx) and poly(2-oxazine)s (POzi) by living cationic ring opening polymerization (LCROP) of 2-substituted 2-oxazolines and 2-substituted 2-oxazines; B) Schematic representation of the amphiphilic triblock copolymers all bearing two hydrophilic poly(2-methyl-2-oxazoline) blocks (blue) and different hydrophobic cores (yellow) as well as their maximum loading capacity (*LC*) for curcumin (CUR).

Small structural changes in the polymer sidechain and polymer backbone of the hydrophobic core caused pronounced differences in the solubilization capacity for different hydrophobic compounds such as curcumin (CUR)[7-9] and paclitaxel (PTX).[10-13] The investigated formulations are of particular interest as extremely high CUR-loading > 50 wt.% were observed, which is highly unusual for drug-loaded micelles, since they generally suffer, with notable exceptions[14, 15], from rather low drug-loadings < 20 wt.%.[16-18] Repeatedly, a stronger hydrophobic contrast resulted in lower drug loadings in this family of amphiphilic block copolymers, clearly stressing the point that the simplistic picture of a hydrophobic core, which dissolves hydrophobic drugs[6], may often be inadequate.[12, 19-21] Since the drug loading (in wt.% vs. polymer) and final drug solubilization (in g/L) are critical parameters dictating, to a certain extent, the clinical potential of a formulation, a closer look at the interactions between polymeric drug carriers and solubilized drug has recently received attention.[21-23] This includes a critical evaluation of the traditional core-shell concept as evident by the drug-induced morphology switch of POx based micelles from worm-like, to spherical and raspberry-like structures with increasing PTX-loading (0 – 50 wt.%)[24, 25]. In contrast, the formation of a worm-like morphology was observed at high-loading (50 wt.%) of the same drug-carrier loaded with etoposide and a platinum (Pt)-based prodrug.[26] It was recently confirmed by Callari *et*. *al*. using solid state nuclear magnetic resonance (NMR) and endocytosis studies[22], that the different morphologies can have direct impact on biological properties.[27] Micelles at low-loading of a Pt-based drug had a rather loose structure, whereas the high-loaded micelles were much more condensed with aggregated Pt-species surrounded by a densely packed hydrophilic corona. The cellular uptake of these micelles, bearing fructose moieties in the hydrophilic corona, depended on fructose-specific cellular uptake transporters. Accordingly, endocytosis was significantly higher at lower loading due to the less-restricted interaction of the flexible polymer chains. In contrast, the apparently too densely packed fructose moieties at higher loading reduced the cellular uptake. Using solid-state NMR, it was recently reported that the hydrophilic corona is also significantly involved in the drug/polymer interactions in POx/POzi micelles, in particular at higher drug loadings, which impeded dissolution of the lyophilized polymer micelle powders, which can be understood as a unusual solid amorphous dispersions.[28] Moreover, using fluorescence spectroscopy and lifetime measurements, significant differences for the molecular environment of the incorporated drug were found at very low drug loading where no involvement of the hydrophilic corona is expected.[13] Inspired by this, we set out to determine if the involvement of the hydrophilic corona in this formulation and distinct polymer-drug specificities observed for POx and POzi based CUR formulations[10] also result in different micellar morphologies or sizes. The analytical techniques utilized so far were not able to address these questions.

To gain extensive insights into the micellar structure, small-angle neutron scattering (SANS) curves of CUR solubilized with three different POx and POzi based amphiphiles (Scheme 1) were obtained at various polymer/CUR ratios. Following this, not only morphological transitions from a distinct core-shell to a core-shell-shell model with increasing CUR-loading could be observed, but also the content of polymer, water or CUR in the different layers could be estimated.

2. MATERIALS AND METHODS

Reagents

Curcumin powder from *Curcuma longa* (turmeric) was purchased from *Sigma-Aldrich* and analyzed in-house (curcumin = 79%; demethoxycurcumin = 17%, bisdemethoxycurcumin = 4%; determined by HPLC analysis). The ABA triblock copolymers, all comprising the same hydrophilic poly(2-methyl-2-oxazoline) (pMeOx) corona A and structurally similar hydrophobic cores based on either poly(2-*n*-2-propyl-oxazine) (pPrOzi; Me-$MeOx_{35}$-$PrOzi_{20}$-$MeOx_{35}$-1-Boc-piperazine =A-pPrOzi-A), poly(2-*n*-2-butyl-oxazoline) (pBuOx; Me-$MeOx_{35}$-$BuOx_{20}$-$MeOx_{35}$-piperidine = A-pBuOx-A) or poly(2-*n*-2-butyl-oxazine) (pBuOzi; Me-$MeOx_{35}$-$BuOzi_{20}$-$MeOx_{35}$-1-Boc-piperazine = A-pBuOzi-A), were synthesized and described previously.[29]

Preparation of CUR-loaded micelles

CUR loaded polymer micelles were prepared by thin film method as described elsewhere.[29] Briefly, ethanolic polymer (20 g/L) and curcumin (5.0 g/L) stock solutions were mixed in the desired ratio. After complete removal of the solvent at 55 °C under a mild stream of argon, the films were dried *in vacuo* (≤ 0.2 mbar) for at least 20 min. Subsequently, preheated (37 °C), ultrapure H_2O was added to obtain the final polymer and CUR concentrations as mentioned in the main text. To ensure complete solubilization, the solutions were shaken at 55 °C for 15 min at 1250 rpm with a Thermomixer comfort (*Eppendorf AG,* Hamburg, Germany). Non-solubilized curcumin, if any, was removed by centrifugation for 5 min at 9.000 rpm with a MIKRO 185 (*Hettich,* Tuttlingen, Germany). CUR quantification was performed by UV-Vis absorption of samples diluted in ethanol using a BioTek Eon Microplate Spectrophotometer (*Thermo Fisher Scientific*, MA, USA) and a calibration curve obtained with known amounts of CUR.[10] For SANS measurements, the freshly prepared aqueous formulations were freeze-dried and redissolved in deuterated water (D_2O) right before measurements. Note that the densimetric measurements were performed in H_2O.

Densimetry

The densimetric measurements were performed using a DMA 4100 M density meter (*Anton Paar*, Graz, Austria). The samples were diluted/dissolved using ultrapure water (H_2O) and the density of each sample was measured from 5 °C to 55 °C. For the estimation of the scattering length densities (SLD) in solution and to calculate the volume fraction, densities obtained at 25°C were used.

Small-angle-neutron-scattering (SANS)

The SANS experiments were performed on the KWS-1 beamline[30] at Heinz Maier-Leibnitz Zentrum (Garching, Germany). The samples were measured in standard Hellma quartz cuvettes with a path-length of 1 mm and kept at 25 °C throughout the experiment. For the measurements, a neutron wavelength of 7 Å was used. To cover the desired Q-range, the samples were measured at three sample to detector distances of 19.6 m, 7.6 m and 1.6 m for 1200 s, 600 s and 300 s respectively. Calibration to absolute intensities was done using poly(methyl methacrylate) (PMMA) as a secondary standard. For data correction, merging and reduction (azimuthal averaging) the toolkit QtiKWS by JCNS was used. The shape model (core-shell-shell sphere) is commonly used and readily available in most software. The model-dependent data analysis was carried out using the macro IRENA for IgorPro.[31]

3. RESULTS AND DISCUSSION

Densimetry

To estimate the volume fractions and neutron scattering length densities (SLD) of polymer-CUR formulations at 25°C (at which SANS experiments were conducted), the densities of the formulations were determined at this temperature. For the complete temperature dependent density data, the reader is referred to supporting information (Figure S1-S6). As expected, the solution density increased with increasing drug concentration (at constant polymer concentration, Table 1).

To derive the density of the polymer-CUR formulations, ρ_{sample}, the amount of water in solution was subtracted:

$$\rho_{sample} = \frac{\rho_{solution}\rho_{water}\, c_{sample}}{\rho_{water} - \rho_{solution}(1 - c_{sample})} \quad (1)$$

with the measured solution density $\rho_{solution}$, the water density ρ_{water} and the total sample mass concentration $c_{sample} = \frac{m_{sample}}{m_{sample}+m_{water}}$, in weight percent. The values for the water density were obtained from calculations at ambient pressure (1013 hPa).[32]

Table 1: Densimetric data of the nanoformulations at different drug loading at 25°C.

polymer/CUR		$\rho_{solution}$ [g/ml][a]	ρ_{sample} [g/ml][b]	ϕ[c]
A-pPrOzi-A				
[g/l]	mmol/mmol			
10/0	n.a.	0.9976	1.0282	0.0091
10/1	1.1/2.7	0.9981	1.0724	0.0096
10/3	1.1/8.1	0.9988	1.1246	0.0109
10/5	1.1/13.6	0.9993	1.1533	0.0122
10/10	1.1/27.1	1.0010	1.2145	0.0154
A-pBuOzi-A				
10/0	n.a.	0.9979	1.0611	0.0094
10/1	1.1/2.7	0.9982	1.0973	0.0095
10/3	1.1/8.1	0.9988	1.1295	0.0108
10/5	1.1/13.6	0.9992	1.1446	0.0123
10/10	1.1/27.1	1.0003	1.1711	0.0160
A-pBuOx-A				
10/0	n.a.	0.9977	1.0389	0.0090
10/1	1.2/2.7	0.9985	1.1211	0.0092
10/3	1.2/8.1	0.9989	1.1530	0.0098
10/5	1.2/13.6	0.9992	1.1708	0.0104

a) measured solution density (system error: 0.0002 g/ml),
b) water subtracted polymer/CUR formulation density (calculated with eq. 1, propagated error: 0.0003)
c) volume fraction (propagated error: 0.0005).

As the polymer and CUR concentrations were ≤ 1 wt.%, it was assumed that the excess volume (polymer & CUR) during mixing of the samples is negligible. The obtained densities of the polymer/CUR formulations were used to calculate the respective volume fractions, ϕ. Here the polymer and CUR concentration can be transformed from weight to volume percent using:

$$\phi\ (\text{vol.}\%) = \frac{\rho_{solution}}{\rho_{sample}}\, c_{sample} \quad (2)$$

The obtained values were used as a fixed fit parameter during the modeling of the SANS data. Using the densities of the pure polymer solutions without any CUR (10-0 samples), the corresponding neutron scattering length densities (SLD_n) of the polymers can be calculated by:

$$SLD_n = \rho \cdot (\textstyle\sum_j n_j b_j)/(\sum_j n_j m_j) \quad (3)$$

where ρ is the macroscopic density, b_j the element- and isotope-specific neutron scattering length, m_j the element specific molecular weight and n_j the stochiometric composition of the compound. For the estimation of the CUR-SLD the density was taken from literature[33] (Table 2).

Table 2: Neutron scattering length densities (SLD) of the polymers, CUR and heavy water (D_2O). The values were calculated from the macroscopic densities using equation (3) or, in case of D_2O, taken from literature[34].

Sample	ρ_{sample} **[g/ml]**	SLD_n [10^{-6} Å^{-2}]
A-pPrOzi-A	1.0282	0.9721
A-pBuOzi-A	1.0611	0.9246
A-pBuOx-A	1.0389	0.9416
CUR	1.30±0.05	1.790
D_2O	---	6.3351

Small-angle neutron scattering

The experimentally determined scattering intensities

$$I(Q) = \textstyle\sum_i F(Q) \cdot \Delta(Q) \cdot\ \mathrm{S}(Q) \quad (4)$$

can be modeled using different form factors, $F(Q)$, size distribution functions, $\Delta(Q)$ and structure factors, $\mathrm{S}(Q)$. In all scattering related theories and experiments, the main variable is always the scattering vector $Q = \frac{4\pi}{\lambda}\sin(\theta)$, which depends on the used wavelength, λ, and the angle, θ, under which the scattered neutrons are collected. The measured SANS data can be used to study the structural properties of the nanoformulations under investigation (Scheme 1).

The scattering curve of pure A-pPrOzi-A in D_2O without any added CUR (A-pPrOzi-A/CUR=10/0, Figure 1, A) shows a flat curve which can be described by the Debye function, indicating a Gaussian chain-like behavior, supporting earlier results, which suggested that this polymer does not form micelles by itself under ambient condition at this concentration (10 g/L).[29] Upon CUR addition, polymer micelles form, as shown by the change in the plateau intensities at low *Q*-values, and the overall appearances of the scattering curves, indicative of discrete and compact objects. The increasing plateau intensity can be caused by larger particles or a higher scattering contrast. A recent report by Lübtow *et al*.[23]

showed that the hydrodynamic radii of A-pPrOzi-A-CUR aggregates initially decrease slightly at low CUR content (10/0.9: hydrodynamic diameter (D_h) = 26 nm; 10-4.8: D_h = 20 nm) and only start to increase at ρ(CUR) > 5 g/L (10/11.9: D_h = 46 nm) as determined by dynamic light scattering (DLS). Since DLS measures the hydrodynamic radius, which involves a water corona around the particle, and SANS probes the radius of gyration without this corona, differences are expected. The increasing scattering intensities probably indicate a higher scattering contrast due to the higher CUR amounts, which is solubilized in the polymer micelles. At 50 wt.% drug loading, i.e. same concentrations of polymer and drug, the scattering intensity increases by nearly an order of magnitude compared to the polymer alone (Figure 1, A and B). The already mentioned DLS results as well as cryo-TEM images[29] have also shown the presence of larger and worm-like particles. These larger structures were also observable by SANS, as the increasing scattering intensities at the lowest measured *Q*-values indicate (Figure 1, D). To investigate these particles in more detail, power-law or model-based fitting techniques could be used. However, for accurate results, either their shape and size or the exact ratio between micelles and larger particles must be known. In the present study, we concentrate on the morphological study of the spherical micelles and hence only the corresponding *Q*-range for single micelles (0.007 - 0.3 Å^{-1}) was considered for further data analysis.

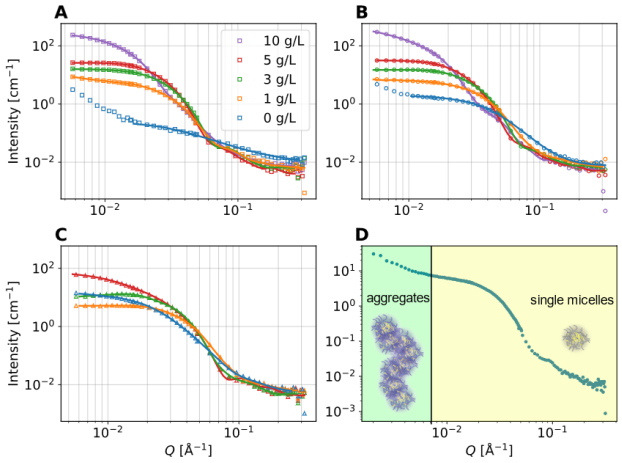

Figure 1: Measured SANS data for A) A-pPrOzi-A, B) A-pBuOzi-A and C) A-pBuOx-A and their CUR nanoformulations. The concentration of the polymer was kept constant at 10 g/L, while the CUR concentration was varied from 0 to 10 g/L. In the case of A-pBuOx-A, CUR concentrations above 3 g/L already caused precipitation. Only one third of the data points is shown to increase visibility. The solid lines are fits to the data obtained by the core-shell-shell model (all fit parameters can be found in the supporting information); D) to show the presence of larger aggregates, the whole data range extended to very small Q-values is shown for A-pPrOzi-A at c(CUR) = 1 g/L (bottom right). The data analysis however, was done on the cropped Q-range shown in the other graphs neglecting those aggregates.

Choice of fitting model

For the analysis of the SANS data, three different spherical form factor models were considered: A simple sphere, a core-shell sphere and a core-shell-shell sphere. Each model is available in the Irena modelling suite and was used to fit the data. The resulting χ^2-values of the best obtained fits were used as an indicator for the most suitable model for data evaluation. A full example and explanation of one sample data set and the fitting results can be found in the supporting information (Figure S7, S8). Based on these results, the core-shell-shell form factor model[31]

$$F(Q) = \frac{3V_1}{QR_1}(\rho_1 - \rho_2)\,J_1(QR_1) + \frac{3V_2}{QR_2}(\rho_2 - \rho_3)\,J_1(QR_2) + \frac{3V_3}{QR_3}(\rho_3 - \rho_0)\,J_1(QR_3) \qquad (5)$$

was chosen and used to fit all data for comparability. Here V_1 to V_3 are the volumes of each compartment (core, first (inner) or second (outer) shell), R_1 to R_3 their respective radii, ρ_1 to ρ_3 the SLD of each compartment, ρ_0 the SLD of the solvent and J_1 is the Bessel function of the first kind. A schematic overview of this model is given in Scheme 2.

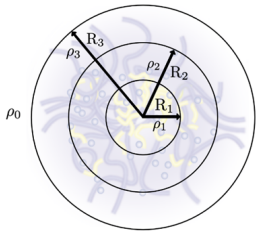

Scheme 2: A graphic representation of the employed core-shell-shell sphere model with its parameters as are defined in Eq. 5.

However, we must note that for several samples the core or one of the shells practically vanish, reducing the model effectively to a simple core-shell model. This may also be attributed to the co-existence of different morphologies, which cryo-TEM images of A-pPrOzi-A formulations suggest and which makes accurate fitting extremely challenging[29].

In addition to the form factor, a structure factor for samples with CUR concentrations above 1 g/L was used for describing the inter-micelle interactions. In the present analysis, the hard sphere structure factor[35-37] was used. This factor assumes a spherically shaped interaction potential between the particles. Hence, the sphere´s diameter, D, and volume fraction of the spheres, ϕ, are not parameters of the micelles, but of the modeled spheres around them, which represent their interaction potential. For the highest CUR concentration (10 g/L), a sticky hard sphere structure factor[35] was used, because sticky micelles and inter-micellar contacts were observed for A-pPrOzi-A/CUR = 10/10 g/L by cryo-TEM[29].

Fit Results

The possible parameter set of the chosen model is rather large including eight (without structure factor) or more fit variables. For reasons of clarity, only the micellar structure defining parameters (size parameters and SLDs) will be shown (Figure 2 and 3). Moreover, to constrain the fitting procedure, it was attempted to match the overall particle size with the results from DLS and cryo-TEM. The full list of model parameters for each sample can be found in the supporting information. As mentioned, A-pBuOzi-A and A-pBuOx-A form micelles without the need of added CUR with critical micelle concentration (cmc) values of 5 mg/L (0.5 µM) and 8 mg/L (1 µM), respectively. Only A-pPrOzi-A needs CUR to form micelles, *i.e.* shows CUR-induced micellization.[29] Hence, there are no values for the core and shell sizes as well as their respective SLDs for pure A-pPrOzi-A in heavy water without any CUR. Obviously, the micellar sizes and structures develop differently in dependence of the CUR-content for all three polymers (Figure 2, 3). Therefore, the different formulations will be evaluated separately in the following. Important to note, the formulation of A-pBuOx-A at polymer/CUR = 10/5 is already above the maximum drug loading, and precipitation occurs. This resulted in very unstable fits in our current work. Therefore, we will not discuss the data analysis of this formulation at this loading any further.

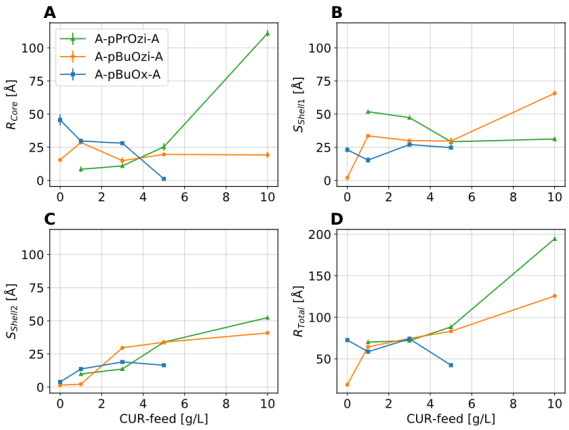

Figure 2: Graphic representation of the micellar size parameters: A) core-radius, B) shell 1 thickness, C) shell 2 thickness and D) total micelle radius. Please note, when size parameters of a particular compartment approach zero, one can consider the resulting morphology again as core-shell instead of core-shell-shell.

A-pBuOzi-A

The core radius of pure A-pBuOzi-A micelles in water is approximately 18 Å (Figure 2, A). Since both shell thicknesses are negligibly small, the observed A-pBuOzi-A aggregates can be described as simple, surprisingly small spheres. Adding CUR (10/1) causes an increase of the micellar core to roughly 30 Å and the development of a first shell with nearly the same size (≈ 35 Å) (Figure 2, B). Increasing the CUR-content (10/3) further, the core of the A-BuOzi-A/CUR-micelles appears to shrink to its initial value and remains almost constant at around 18-20 Å upon further increase of CUR. The first (inner) shell remains at the same size as well for intermediate CUR loadings, but a second, outer shell becomes noticeable for a CUR-concentration of 3 g/L, which has nearly the same size as the first shell (Figure 2, C). This shell also increases slightly in size with increasing CUR feed.

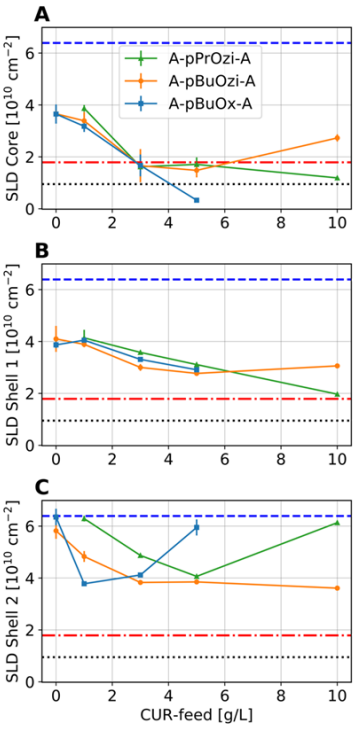

Figure 3: Graphic representation of the fitted SLDs of A) the micelles core, B) its first shell and C) second shell. Additionally, the SLDs of heavy water (blue dashed line), CUR (red dash-and-dot line) and the polymers (black dotted line) are marked.

At maximum loading (10/10), another notable change of the A-pBuOzi-A micelles is observed with the thickness of shell 1 doubling in size to approximately 60 Å. In general, we found that the data analysis at CUR concentrations of 10 g/L with only one fitting model was very challenging. Our fit describes the vast majority of the particles in solution. Additional particles at lower concentrations can only be described with better *a priori* knowledge about their size and shape.

Apart from the size, further insights into the actual composition of the different micellar layers can be obtained from the fitted SLDs (Figure 3). Pure A-pBuOzi-A (CUR = 0 g/L) forms spherical aggregates with no core-shell differentiation. The fitted SLD is approx. 3.6×10^{-6} Å^{-2} and therefore almost perfectly in between the SLDs of A-pBuOzi-A and D_2O (Table 2), suggesting that the ratio of A-pBuOzi-A/D_2O is roughly 1/1. In other words, these micelles do not exhibit a core-shell structure but are rather homogenous in composition, which we tentatively attribute to excellent hydration of the hydrophobic repeat units by virtue of the polar and flexible poly(2-oxazine) backbone. By adding CUR (CUR = 1 g/L), SLD_{core} decreases slightly (Figure 3, A), which could be an indication of the dehydration of the core in favor of CUR inclusion. The SLD of the first shell is slightly above the initial value of the spherical aggregates (roughly 4×10^{-6} Å^{-2}) (Figure 3, B), which hints towards a A-pBuOzi-A/D_2O mixture with a slightly higher D_2O-fraction. The second, very small, shell contains almost only D_2O as judged by the SLD (Figure 3, C). Being very small and essentially D_2O, this second shell is negligible. With increasing CUR concentration, the SLDs of the core and both shells decrease indicating further dehydration. After reaching a CUR concentration of 3 g/L, the SLDs of the system remain almost constant. This indicates a possibly stable composition in every part of the micelle. According to the SLDs, it appears as though CUR is mostly present in the core. At the highest possible CUR concentration of 10 g/L, the morphological situation is somewhat similar to the situation without CUR, as the composition of all components appears to be quite similar, according to the SLDs (Figure 3). Accordingly, we cannot consider the micelles anymore as core-shell-shell structure but rather a large homogenous sphere. A similar distribution of CUR into the outer, hydrophilic shell of glycopolymers was previously observed by Stenzel and coworkers using SANS.[23] Increasing amount of CUR dehydrated the nanoparticle shell, which coincided well with a lower cellular uptake of the respective nanoparticles.

A-pBuOx-A

In contrast to A-pBuOzi-A, neat A-pBuOx-A micelles have a core-shell structure and are significantly larger than the A-pBuOzi-A assemblies at the same concentration with a total radius of approximately 75-80 Å (Figure 2, D). However, the SLDs of the core and this shell are also very similar (Figure 3, A and B). Again, the size of the second shell is negligible, resulting in an overall core-shell structure (Figure 2, C). This seems inconsistent as BuOzi should be more hydrophobic than BuOx, and thus, a stronger core-shell contrast would be expected. However, preliminary comparison of ^{1}H-NMR spectra in $CDCl_3$ and D_2O indeed suggest a highly hydrated and thus mobile BuOzi core, but this will have to be studied separately in more detail.

In contrast to the other two polymers, A-pBuOx-A micelles seem to shrink in size in the presence of CUR. At a CUR concentration of 1 g/L, the overall size of the micelles reduces to approximately 60 Å, even though a second shell becomes apparent (Figure 2, C and D). This can be explained by splitting of the initial shell into shell 1 and shell 2. Therefore, the thickness of the first shell is reduced by half and also the core size is reduced (Figure 2, A and B). Such a compaction of the aggregate structure could be a hint towards

strong polymer-CUR interactions. Interestingly, stronger drug-polymer interactions were recently suggested in the system A-pBuOx-A/CUR compared to A-pPrOzi-A/CUR by fluorescence up-conversion studies.[13] Although A-pPrOzi-A enables extremely high CUR-loadings up to 54 wt.%, in contrast to 24 wt.% of A-pBuOx-A[10], at low loading, the molecular mobility of CUR within A-pBuOx-A was lower than in A-pPrOzi-A. This was interpreted with stronger, more defined A-pBuOx-A/CUR interactions, whereas CUR seemed to be more loosely incorporated into A-pPrOzi-A.

With increasing CUR loading (10/3), the core size of A-pBuOx-A remains nearly constant while the first and second shell thickness slightly increases for the nanoformulations. This is in contrast to the other to polymer, where core slightly increases at this point.The total micelle radius approaches again 80 Å (Figure 2, D). Above this concentration, CUR starts to precipitate, which results in the failure of the fitting model, since more than one particle population is present in solution. Considering the SLD values, the core and first shell are heavily and almost equally well hydrated in the absence of CUR (Figure 3, A and B). The second shell of negligible size consists only of D_2O (Figure 3, C). At low loading (10/1), fitting revealed that the first and second shell exhibit same SLD-values and therefore should have a similar composition. Therefore, a simple core-shell morphology can be assumed. This is an indication of a dehydration of the core and the second shell. The lower core SLD can be explained by the presence of CUR, while the SLD reduction of the second shell could result from a higher polymer content. This is in good agreement with the overall smaller micellar size, and significantly reduced core size (Figure 2, A and D). Further increasing the CUR concentration to 3 g/L, the core SLD reduces to a point, where it can be assumed that the core is almost entirely consisting of CUR and A-pBuOx-A with little to no D_2O left (Figure 3, A). The SLD of the first shell reduces as well, while the SLD of the second shell increases (Figure 3, C and D). This could again indicate an incorporation of CUR in the first shell and increasing D_2O fraction in the outer shell.

A-pPrOzi-A

At a CUR concentration of 1 g/L, A-pPrOzi-A exhibits a pronounced core-shell-shell structure with a relatively small core and outer shell, but very big first shell (Figure 2). The total micelle radius is roughly 70-80 Å (Figure 2, D), which is in reasonably good agreement with data from DLS.[29] With increasing CUR concentrations, both the core and outer shell grow, while the inner shell shrinks. Reaching a CUR concentration of 10 g/L, the core dimension increases very profoundly, which is in line with data from DLS[29].

The SLDs of all A-pPrOzi-A-micelle parts decrease with increasing CUR concentration (Figure 3). Starting from a highly hydrated core and first shell, it is quickly evident that the largest amount of CUR is stabilized in the core of the micelles, since the SLDs of the core decrease much steeper and the SLD stabilizes in between the SLDs of pure CUR and A-pPrOzi-A (Figure 3, A). The involvement of the first shell in the solubilization of CUR is clearly evidenced by its SLD, which is smaller than the one of the second shell (Figure 3, B and C). The SLD of the large core corroborates a mixture of CUR and polymer. The relatively thin first shell remains hydrated as evident by a larger SLD value. The second shell vanishes again at this point as the SLD is essentially that of pure D_2O.

CUR spatial distribution at different loadings

Using the fitted sizes of each micelle section (Figure 2) and their respective SLDs (Figure 3), it is possible to estimate the amount of CUR, which is present in the respective component, *i.e.* the micellar core and shell. In this regard, the method established by Stenzel *et al.*[22, 23] was used and modified. Since each micelle component can comprise polymer, CUR and D_2O, the fitted SLD can be written as

$$SLD_{Fit} = \phi_{polymer} \cdot SLD_{polymer} + \phi_{CUR} \cdot SLD_{CUR} + \phi_{D_2O} \cdot SLD_{D_2O}$$

with the volume fraction in each micelle component ϕ and the calculated $SLDs$ of polymer, CUR and D_2O (Table 2). Additionally, the two boundary conditions

$$\phi_{polymer} + \phi_{CUR} + \phi_{D_2O} = 1,$$

$$\phi_{CUR}^{Core} + \phi_{CUR}^{shell1} + \phi_{CUR}^{shell2} = LC$$

can be used, where the loading capacity $LC = \frac{V_{CUR}}{V_{polymer}+V_{CUR}}$ constrains the total amount of CUR in the micelle. The extremely high values for *LC* were determined experimentally and are already reported by Lübtow *et al.*[10] The following assumptions were made for the calculation of ϕ_{CUR}: Firstly, the second shell never incorporates any CUR, which may however not be entirely correct. Secondly, the D_2O amount in the core is negligible for all CUR concentrations. The last assumption guarantees a solvable equation system. If the CUR amount in the core is not sufficient for obtaining the measured loading capacity, the CUR amount in the first shell will be increased accordingly. The resulting CUR volume fractions ϕ_{CUR} of the core and the first shell show a clear trend for all three polymers (Figure 4).

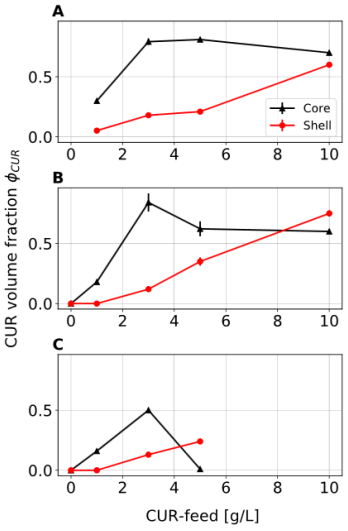

Figure 4: Calculated CUR volume fractions using the fitted SLDs of the core and first shell (Figure 3) for A) A-pPrOzi-A, B) A-pBuOzi-A and C) A-pBuOx-A. The total volume fraction was constrained by the sum of both ϕ_{CUR} of the core and first shell being identical to the reported loading capacities[29]. Here, the volume of each micelle section (core and shell 1) was calculated using the structural parameters shown in Figure 3.

Additionally, the results are summarized and sketched in Figure 5. While the core mainly receives CUR at low [CUR]=1-3 g/L, the first shell must include small amounts of CUR here as well to obtain the measured LC. With increasing CUR feed, both core and shell 1 incorporate more CUR. ϕ_{CUR} in the shell reaches estimated values of up to 20-30% for all three polymers (3 and 5 g/L). Only at high polymer concentrations, the values for ϕ_{CUR} become less reasonable and trustworthy, since the nanoformulations either aggregated and precipitated (A-pBuOx-A) or the particle shape becomes more heterogenetic due to the presence of larger agglomerates or

worm-like structures (A-pPrOzi-A and A-pBuOzi-A). Nevertheless, the analysis of SANS data unambiguously shows that the micellar shell is involved in incorporating large amounts of CUR and plays an essential role in the stabilization process. This corroborates recent finding, where solid-state NMR spectroscopy also revealed interaction of CUR with the amide moieties in the hydrophilic corona of A-pPrOzi-A which lead to a decrease in dissolution rates at higher loadings.[28] In addition, when the hydrophilic blocks were exchanged to the slightly less hydrophilic poly(2-ethyl-2-oxazoline), solubilization capacity of the corresponding ABA triblock copolymers for CUR and paclitaxel drastically decreased.[38] Similarly, stabilization of CUR and paclitaxel using a methacrylate based system featuring fructose containing corona forming blocks has also been previously reported.[22, 23]

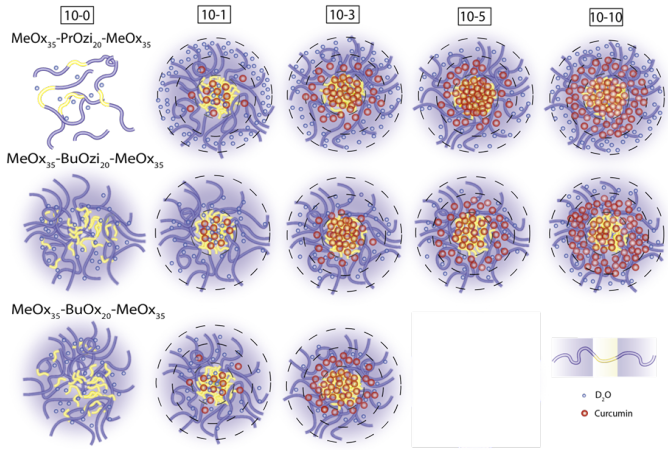

Figure 5: Schematic illustration of the different micellar morphologies at various CUR contents shown in Figure 5. The sizes of the micelle compartments are not to scale to facilitate comparability. To visualize the amount of CUR in each micellar section, the number of red dots roughly represents the respective CUR concentration.

4. CONCLUSION

Poly(2-oxazoline)/poly(2-oxazine) based micelles have been shown to be highly unusual as they enable extraordinary high drug loading of more than 50 wt.% in select cases. Increasing experimental evidence suggests that this high drug loading is intimately linked with interactions of the drug with the hydrophilic corona. Here, we investigated the influence of the loading of three different but structurally similar ABA triblock copolymers with the model compound curcumin on the morphology of the resulting micelles. While without CUR no pronounced core shell character was found, addition of small amounts of CUR enhanced the contrast between core and corona. In all cases, CUR concentrated in the core at low drug loadings. With increasing CUR concentrations, the picture becomes more complicated and the scattering data could not be reasonably fitted using the previously employed core-shell model. Our data suggests a core-shell-shell morphology, with parts of the hydrophilic corona filling up with CUR and effectively forming a second, inner shell, while the other shell remains hydrated and colloidally stabilizes the micelles. With more CUR added, this situation eventually becomes unstable, finally causing precipitation. This happens already at about 25 wt.% drug loading for the A-pBuOx-A micelles, while those with poly(2-oxazine) based B block allow overall drug loading of 50 wt.%. The insufficient difference in scattering length density between the hydrophilic and hydrophobic block of the studied block copolymers made hampered a more detailed analysis of the presently investigated systems. However, to overcome this limitation will require block copolymer, in which the different blocks are deuterium labeled.

Acknowledgments

Financial support by the Deutsche Forschungsgemeinschaft is gratefully acknowledged (Project number 398461692, awarded to R.L.). The authors thank JCNS for allocating beamtime (proposal #12083) and providing excellent equipment and support, before, during and after the beam-time. Also, we appreciate valuable feedback by Ann-Christin Pöppler. M.M.L. would like to thank the Evonik Foundation for providing a doctoral fellowship.

References

[1] E. M. Merisko-Liversidge, G. G. Liversidge, *Toxicol. Pathol.* **2008**, *36*, 43-48.

[2] C. Giliyar, D. Fikstad, S. Tyavanagimatt, *Drug Deliv. Technol* **2006**, *6*, 57-63.

[3] H. D. Williams, N. L. Trevaskis, S. A. Charman, R. M. Shanker, W. N. Charman, C. W. Pouton, C. J. H. Porter, *Pharmacol. Rev.* **2013**, *65*, 315.

[4] H. Cabral, K. Miyata, K. Osada, K. Kataoka, *Chem. Rev.* **2018**, *118*, 6844-6892.

[5] J. Liu, Y. Xiao, C. Allen, *J. Pharm. Sci.* **2004**, *93*, 132-143.

[6] A. O. Kasimova, G. M. Pavan, A. Danani, K. Mondon, A. Cristiani, L. Scapozza, R. Gurny, M. Möller, *J. Phys. Chem. B* **2012**, *116*, 4338-4345.

[7] M. A. W. Jonathan Baell, *Nature* **2014**, *513*, 481-483.

[8] M. Heger, *Nature* **2017**, *543*, 40-40.

[9] S. C. Gupta, S. Patchva, B. B. Aggarwal, *AAPS J.* **2013**, *15*, 195-218.

[10] M. M. Lübtow, L. Hahn, M. S. Haider, R. Luxenhofer, *J. Am. Chem. Soc.* **2017**, *139*, 10980-10983.

[11] Y. Seo, A. Schulz, Y. Han, Z. He, H. Bludau, X. Wan, J. Tong, T. K. Bronich, M. Sokolsky, R. Luxenhofer, R. Jordan, A. V. Kabanov, *Polym. Adv. Technol.* **2015**, *26*, 837-850.

[12] M. M. Lübtow, M. S. Haider, M. Kirsch, S. Klisch, R. Luxenhofer, *Biomacromolecules* **2019**, *20*, 3041-3056.

[13] M. M. Lübtow, H. Marciniak, A. Schmiedel, M. Roos, C. Lambert, R. Luxenhofer, *Chem.: Eur. J.* **2019**, *25*, 12601-12610.

[14] Y. Milonaki, E. Kaditi, S. Pispas, C. Demetzos, *J. Polym. Sci. Pol. Chem.* **2012**, *50*, 1226-1237.

[15] Y. Zhang, T. Ren, J. Gou, L. Zhang, X. Tao, B. Tian, P. Tian, D. Yu, J. Song, X. Liu, Y. Chao, W. Xiao, X. Tang, *J. Control. Release* **2017**, *261*, 352-366.

[16] O. Naksuriya, S. Okonogi, R. M. Schiffelers, W. E. Hennink, *Biomaterials* **2014**, *35*, 3365-3383.

[17] R. Raveendran, K. M. Mullen, R. M. Wellard, C. P. Sharma, R. Hoogenboom, T. R. Dargaville, *Eur. Polym. J.* **2017**, *93*, 682-694.

[18] S. Datta, A. Jutková, P. Šrámková, L. Lenkavská, V. Huntošová, D. Chorvát, P. Miškovský, D. Jancura, J. Kronek, *Biomacromolecules* **2018**, *19*, 2459-2471.

[19] M. M. Lübtow, L. Keßler, A. Appelt-Menzel, T. Lorson, N. Gangloff, M. Kirsch, S. Dahms, R. Luxenhofer, *Macromol. Biosci.* **2018**, *18*, 1800155.

[20] L. M. Johnson, Z. Li, A. J. LaBelle, F. S. Bates, T. P. Lodge, M. A. Hillmyer, *Macromolecules* **2017**, *50*, 1102-1112.

[21] Z. Li, T. I. Lenk, L. J. Yao, F. S. Bates, T. P. Lodge, *Macromolecules* **2018**, *51*, 540-551.

[22] C. Cao, J. Zhao, M. Lu, C. J. Garvey, M. H. Stenzel, *Biomacromolecules* **2019**, *20*, 1545-1554.
[23] C. Cao, J. Zhao, F. Chen, M. Lu, Y. Y. Khine, A. Macmillan, C. J. Garvey, M. H. Stenzel, *Chem. Mater.* **2018**, *30*, 5227-5236.
[24] A. Schulz, S. Jaksch, R. Schubel, E. Wegener, Z. Di, Y. Han, A. Meister, J. Kressler, A. V. Kabanov, R. Luxenhofer, C. M. Papadakis, R. Jordan, *ACS Nano* **2014**, *8*, 2686-2696.
[25] S. Jaksch, A. Schulz, Z. Di, R. Luxenhofer, R. Jordan, C. M. Papadakis, *Macromol. Chem. Phys.* **2016**, *217*, 1448-1456.
[26] X. Wan, Y. Min, H. Bludau, A. Keith, S. S. Sheiko, R. Jordan, A. Z. Wang, M. Sokolsky-Papkov, A. V. Kabanov, *ACS Nano* **2018**, *12*, 2426-2439.
[27] M. Callari, P. L. De Souza, A. Rawal, M. H. Stenzel, *Angew. Chem. Int. Ed.* **2017**, *56*, 8441-8445.
[28] A.-C. Pöppler, M. M. Lübtow, J. Schlauersbach, J. Wiest, L. Meinel, R. Luxenhofer, *Angew. Chem. Int. Ed.* **2019**, doi:10.1002/anie.201908914.
[29] M. M. Lübtow, L. C. Nelke, J. Seifert, J. Kühnemundt, G. Sahay, G. Dandekar, S. L. Nietzer, R. Luxenhofer, *J. Control. Release* **2019**, *303*, 162-180.
[30] A. V. Feoktystov, H. Frielinghaus, Z. Di, S. Jaksch, V. Pipich, M.-S. Appavou, E. Babcock, R. Hanslik, R. Engels, G. Kemmerling, H. Kleines, A. Ioffe, D. Richter, T. Bruckel, *J. Appl. Cryst.* **2015**, *48*, 61-70.
[31] J. Ilavsky, P. R. Jemian, *J. Appl. Cryst.* **2009**, *42*, 347-353.
[32] National Institute of Standards and Technology (NIST) Chemistry WebBook (SRD 69), Thermophysical Properties of Fluid Systems, https://webbook.nist.gov/chemistry/fluid/ (accessed June 2019).
[33] S. Balasubramanian, A. M. Mohite, K. K. Singh, T. J. Zachariah, T. Anand, *JOSAC* **2012**, *21*, 178-181.
[34] V. F. Sears, *Neutron News* **1992**, *3*, 26-37.
[35] S. Kline, *J. Appl. Cryst.* **2006**, *39*, 895-900.
[36] B. Hammouda, *Probing Nanoscale Structures – The SANS Toolbox, Vol. chapter 32 - Structure factors for particulate systems*, National Institute of Standards and Technology (NIST), Center for Neutron Research, Gaithersburg, **2016**.
[37] J. K. Percus, G. J. Yevick, *Phys. Rev.* **1958**, *110*, 1-13.
[38] M. S. Haider, M. M. Lübtow, S. Endres, V. Aseyev, A.-C. Pöppler, R. Luxenhofer, *ChemRxiv* **2019**, https://doi.org/10.26434/chemrxiv.9710579.v9710571.